Appl. Phys. A 79, 729–734 (2004)
DOI: 10.1007/s00339-004-2644-8

Applied Physics A
Materials Science & Processing

N. ARNOLD✉
G. SCHREMS
D. BÄUERLE

Ablative thresholds in laser cleaning of substrates from particulates

Angewandte Physik, Johannes-Kepler-Universität, 4040 Linz, Austria

Received: 26 September 2003 / Accepted: 4 February 2004
Published online: 26 July 2004 •

ABSTRACT 'Laser cleaning' thresholds based on the local ablation of substrate material are studied theoretically. Results are compared with the experimental data on the cleaning of silicon wafers from spherical silica particles using laser wavelengths at 248, 532 and 1064 nm. Calculations take into account local enhancement in the laser-light intensity and are based on analytical solutions for the temperature distribution. Influence of vapor atmosphere on cleaning thresholds is studied experimentally and theoretically. Here cleaning is assisted by explosive vaporization of capillary condensed water. A possibility to increase the window for damage-free cleaning by varying the pulse duration and laser wavelength is also discussed.

PACS 42.62.Cf; 81.65.Cf; 68.35.Np

1 Introduction

Dry laser cleaning (DLC) is a single-step method of sub-μm particle removal from surfaces [1]. Earlier models of DLC considered mechanisms based on the one dimensional (1D) thermal expansion [2–4]. Field enhancement near the particle leads to a local temperature rise and to three-dimensional (3D) thermal expansion near the particulate [5–7]. This yields more realistic theoretical thresholds [8], but still cannot describe experimental threshold fluences over the broad range of particle radii.

At the same time, experiments often reveal damage at the positions of removed particles [7, 9–11]. In certain cases, this damage seems to be a prerequisite for cleaning. We consider laser cleaning based on local ablation and explore expected dependence of the cleaning fluence ϕ_{cl} on particle radius r. Besides, we consider the influence of capillary condensed water and discuss the possibility to avoid damage using longer absorption lengths in the substrate.

2 Overview of optical field enhancement

Transparent spherical particles, (silica, polystyrene (PS), etc.) are often used in laser cleaning experiments to get well-defined and reproducible conditions [2, 3, 5, 7, 9, 10].

✉ Fax: +43-732/2468-9242, E-mail: nikita.arnold@jku.at

The exact distribution of the scattered field can be calculated only numerically [9–11]. In general, small particles with radii $r < \lambda$ behave like dipoles (subscript 'd'), with polarizability proportional to their volume. This leads to an additional 3D intensity contribution $M_{\mathrm{d}} \propto (kr)^2$ underneath the particle. Here $k = 2\pi/\lambda$ is the wave-number and kr the Mie parameter. The width of the intensity enhanced region is $w_{\mathrm{d}} \sim r$. Transparent spheres with $r \gg \lambda$ act as aberrated lenses. According to geometrical optics (subscript 'g') the intensity is confined within a cone of radius w_{g}. The caustic surface of this cone has higher intensity than its interior. Besides, saggital rays intersect on the symmetry axis, creating a caustic line (subscript 'c'). As a result, the central intensity under the particle is comparable with that in the aberrated focus and localized within a radius w_{c}. Figure 1 shows the caustic line in the center, the caustic ring, and the geometrical region, which contains the largest fraction of the total power.

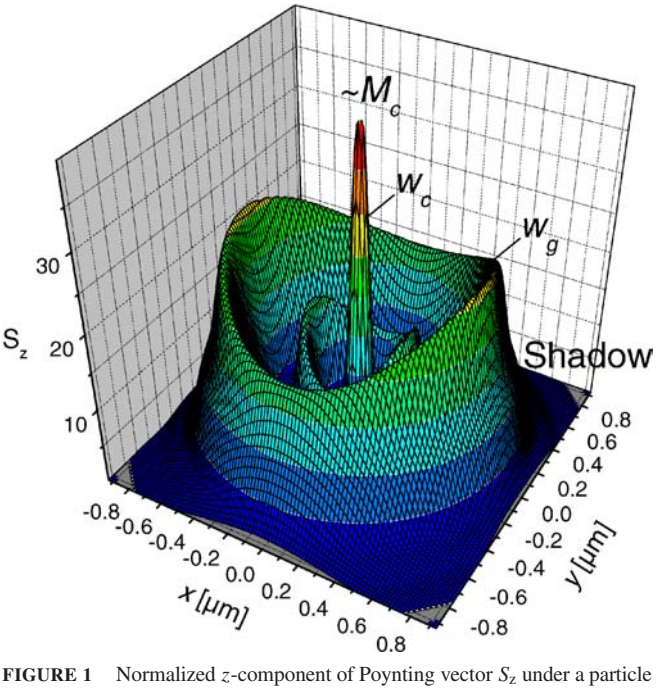

FIGURE 1 Normalized z-component of Poynting vector S_z under a particle of radius $r = z = 3.1$ μm, $n = 1.4$, $\lambda = 248$ nm. Mie parameter $kr = 78.54$. The peak M_{c} in the center originates from the central caustic line with the width w_{c} . w_{g} is the width of caustic cone

	Central line	Caustic cone	Geom. region	Abber. focus	Ideal focus
Width b	$k^{-1}\sim\lambda$	$\lambda^{2/3}r^{1/3}$	r	$\lambda^{3/4}r^{1/4}$	$k^{-1}\sim\lambda$
Area s	$k^{-2}\sim\lambda^2$	$\lambda^{2/3}r^{4/3}\sim br$	r^2	$\lambda^{3/2}r^{1/2}$	$k^{-2}\sim\lambda^2$
Intensity I	kr	$(kr)^{1/3}$	const	kr	$(kr)^2$
Power $P\sim Is$	λr	$\lambda^{1/3}r^{5/3}$	r^2	$\lambda^{1/2}r^{3/2}$	r^2
P fraction	$(kr)^{-1}$	$(kr)^{-1/3}$	const ~ 1	$(kr)^{-1/2}$	const ~ 1
Stationary $T\sim Ib\sim P/b$	r	$\lambda^{1/3}r^{2/3}\sim Ir$	r	$\lambda^{-1/4}r^{5/4}$	$\lambda^{-1}r^2$

TABLE 1 Asymptotic behavior of the enhanced intensity under the large transparent spheres

Table 1 (deduced from [12]) summarizes the different contributions to the energy that 'flows' through the particle. Which contribution determines local ablation threshold depends on the laser pulse duration τ. For ps pulses the radial heat conduction is negligible, and the onset of ablation will be determined by the highest intensity in the center. For ns pulses the intensity distribution will be smeared out and the overall average intensity is important. We describe this by an equivalent Gaussian beam, though the actual intensity is larger near the circumference.

There exist finer effects, related to waves undergoing total internal reflection within the spheres. Evanescent tails of these waves contribute to the intensity distribution in the near field. They are stronger if certain (Mie) resonance conditions are met [3, 7]. However, such effects are difficult to observe due to dispersion in particle sizes, absorption and deformations. The subsequent treatment neglects the effect of Mie resonances and describes the average behavior of slightly different particles [8]. To derive general trends, we will use the semi-empirical approximation

$$I(\varrho)=I_0\left[1-S\exp(-\varrho^2/w_{\rm sh}^2)+M\exp(-\varrho^2/w^2)+M_{\rm c}\exp(-\varrho^2/w_{\rm c}^2)\right] \quad (1)$$

where ϱ is the radial coordinate. The first term refers to homogeneous irradiation. The second term refers to the shadow under the particle [7, 8]. It disappears for small particles, due to the size-dependent coefficient S that changes from 0 to 1 in the region where the geometrical optics becomes relevant [6].

$$S=\frac{C(kr)^2}{1+C(kr)^2}\quad\text{with } C=\frac{n^2-1}{n^2+2}\sqrt{\frac{(4-n^2)^3}{27n^4}};\ w_{\rm sh}=r+\lambda\,. \quad (2)$$

The third term combines dipole and geometrical optics enhancements [6].

$$M\approx\frac{M_{\rm d}M_{\rm g}}{M_{\rm d}+M_{\rm g}}\quad\text{with}\quad M_{\rm d}=2\frac{n^2-1}{n^2+2}(kr)^2 \quad\text{and}\quad M_{\rm g}=\frac{27n^4}{(4-n^2)^3}-1 \quad (3)$$

$$w=\frac{w_{\rm d}+C(kr)^2w_{\rm g}}{1+C(kr)^2}\quad\text{with}\quad w_{\rm d}=r \quad\text{and}\quad w_{\rm g}=r\sqrt{\frac{(4-n^2)^3}{27n^4}}\,. \quad (4)$$

The last term in (1) refers to the central caustic line under the sphere and disappears for small kr. From the asymptotic (Table 1) and the comparison with the numerical investigations based on Mie formulas [8] we choose:

$$M_{\rm c}=2(n-1)krS\quad\text{and}\quad w_{\rm c}=\lambda/5. \quad (5)$$

The empirical coefficient $2(n-1)$ gives reasonable numbers over the broad range of sizes. All these approximations work for weakly absorbing spheres with $1.1<n<1.8$ and for the intensity understood as z-component of the Poynting vector [8].

Figure 2 shows the contributions of different terms in (1) and compares them with the averaged Mie results from [8]. With small particles the temperature rise is dominated by 1D contribution. With micron-sized particles, the highest intensity is reached in the central caustic line. However, the main contribution to the temperature still comes from the geometrical part due to its larger total fraction of power (see Table 1). Only for very large particles the maximum temperature is due to the caustic line in the center.

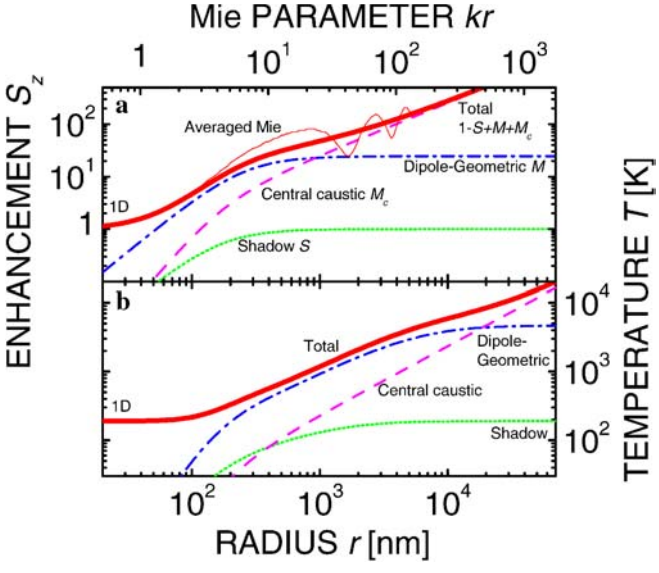

FIGURE 2 Contribution of different terms in (1) to intensity (**a**) and temperature (**b**). *Dotted curve* – shadow S; *dash-dotted curve* – dipole-geometrical contribution M; *dashed curve* – central caustic spot $M_{\rm c}$; *solid curve* – total central intensity $1-S+M+M_{\rm c}$; *thin solid curve* in **a** – exact averaged Mie result for S_z [8]; Refractive index $n=1.5$. Temperature rise in **b** refers to $\phi=0.1\,{\rm J/cm^2}$ and the parameters of KrF laser

3 Temperature calculations

The central temperature rise induced in the substrate by each of the Gaussian terms in (1) can be estimated from the expression (7.5.1) in [1] convoluted with the temporal pulse profile $I(t)$. Material parameters are assumed to be constant and their definitions and values are listed in Table 2. The other parameters are the same as those in [13]. For the thermal diffusivity and absorption coefficient of Si average values that correctly predict the homogeneous melting threshold were used. Measured threshold values are included in Table 2. The particle temperature was estimated by neglecting any thermal contact with the substrate (ref. [7]) and using the absorption cross-section $\sigma_a \approx \frac{4}{3}\pi r^3 \frac{\alpha_p}{n}\left[n^3-(n^2-1)^{3/2}\right]$ from [14]. Bulk quartz is rather transparent at wavelengths under study. However, one cannot exclude the influence of an elevated hydrogen content in colloidal particles and/or the existence of surface states.

4 Conditions for ablative cleaning

When the local temperature under the particle becomes high enough, evaporation starts. This results in momentum transfer and removal of the particle. It is difficult to define the exact threshold conditions for such a process, due to uncertainties in the geometry of the heated region and high-temperature values of parameters. However, the ablation rate obeys an Arrhenius law [1]. Near threshold, evaporation consumes a small fraction of the absorbed laser energy and the temperature is about proportional to the laser fluence. Thus, the ablated volume and the pressure of the vapor increases sharply in a narrow interval of fluences. This makes the exact ablation temperature used in the estimations unimportant. With ns laser pulses, significant ablation requires temperatures around $1.5T_b$ to be reached. For typical numbers, 10% increase in temperature near $1.5T_b$ (T_b is a boiling point of material (see Table 2) increases the ablation rate and the pressure tenfold (from 100 to 1000 bar [1]). Estimations show, that such pressures easily overcome adhesion forces, though vaporization of material in the contact area may eliminate adhesion completely.

5 Experimental

Cleaning was performed either in vacuum or in water vapor. A KrF laser (Lambda Physik LPX 205, 28 ns FWHM) or a Nd : YAG laser (Continuum Surelight I-20, 6 ns FWHM) were used. The KrF laser allowed homogenous irradiation with fluences up to 0.5 J/cm^2. The pulse energy was tuned by an adjustable dielectric attenuator. A beam splitter placed between the attenuator and target, enabled in situ measurement of the pulse energy. The Nd : YAG laser beam required homogenization. Two options were used. 1) A quartz rod produces high homogeneity, but limits the maximum fluence at 0.5 J/cm^2. 2) An aluminum waveguide results in lower homogeneity, but allows fluences up to 1.5 J/cm^2.

Vacuum DLC was performed in a chamber evacuated for three hours and heated to $37.7 \pm 0.5°$ prior to irradiation, to remove residual moisture. During irradiation, the pressure inside the chamber was always below 2×10^{-4} mbar. The storage time was shorter than 24 hours for particles with $2r < 1500$ nm, and shorter than six hours for particles with 3280 nm and 5000 nm diameter.

Cleaning in water atmosphere was performed in a chamber with a relative humidity (*RH*) between 94% and 97%, a pressure between 31 mbar and 37 mbar and a temperature between 23.5 °C and 27.5 °C. The partial pressure of other gases was lower than 1 mbar.

The cleaning efficiency was determined by counting the particles with a digitizing software. Pre-irradiated and a post-irradiated picture of the same area on the wafer were compared. This allowed for the detection of low cleaning efficiencies. Single-pulse cleaning thresholds ϕ_{cl} were determined from the fit of the cleaning efficiency plots in the linear range.

Pulse duration τ in $I(t) = I_0 \frac{t}{\tau} \exp(-\frac{t}{\tau})$	11 ns (27 ns FWHM) KrF, 248 nm 3.27 ns (8 ns FWHM) SH Nd : YAG, 532 nm 3.27 ns (8 ns FWHM) Nd : YAG, 1064 nm
Substrate c-Si	
Thermal Diffusivity D_s	0.32 cm^2/s
Melting point T_{ms}	1690 K
Temperature to reach 300 bar	$\approx 1.43\, T_{bs} = 1.43 \times 2654$ K $= 3795$ K
Speed of sound v_0	0.93×10^6 cm^2/s
Absorption coefficient α_s	1.67×10^6 cm^{-1} KrF, 248 nm [1] 1×10^5 cm^{-1} SH Nd : YAG, 532 nm at 1000 K 5.8×10^2 cm^{-1} Nd : YAG, 1064 nm (averages that give right melting thresholds)
Absorptivity A_s	0.39 KrF, 248 nm [1] 0.63 SH Nd-YAG, 532 nm [1] 0.7 Nd-YAG, 1064 nm [1]
Reported (calculated) homogeneous melting threshold ϕ_m	0.725 [19] (0.729) J/cm^2 KrF, 248 nm 0.28 [7] p. 164, (0.283) J/cm^2 SH Nd : YAG, 532 nm ~ 6 [1] p. 176, (5.98) J/cm^2 Nd : YAG, 1064 nm
Particle SiO_2	
Melting point T_{mp}	1873 K
Temperature to reach 300 bar	$\approx 1.54 T_{bp} = 1.54 \times 2503$ K $= 3854$ K
Absorption coefficient α_p	$1. \times 10^3$ cm^{-1}
Refractive index n	1.5
Critical temperature, water T_{cl}	647 K

TABLE 2 Parameters used in the calculations

6 Comparison of experimental data and calculations

Theoretical and experimental cleaning thresholds are compared in Fig. 3. Figure 3a refers to KrF radiation. 3D thermal expansion is largely due to dipole-geometric term M in (1). Caustic contribution to the thermal expansion is small due to its small spatial scale.

The slope of $\phi_{\rm cl}(r)$ curves predicted by the thermal expansion model (dashed curve) is too high. The slopes for the $\phi_{\rm cl}$ defined as the condition to reach substrate melting temperature $T_{\rm ms}$, (dash-dotted curve) or $1.5T_{\rm bs}$ (solid curves) are about equal and agree well with the slope revealed by the experimental results. The thick solid curve was calculated with the approximation (3)–(5), while thin solid and dash-dotted curves in the 'dipole' region used more accurate averaged Mie results from Fig. 2. With larger particles the discrepancy with the Mie results is due to oscillations in the intensity of the central caustic line, which almost does not influence temperature (see Fig. 2). The agreement in values of $\phi_{\rm cl}(r)$ is better if one uses $T_{\rm ms}$ as a threshold condition (dash-dotted curve, which also uses Mie results in the dipole region). This fact seems to be accidental and can be tentatively attributed to the approximations. Among those are: influence of the substrate, which may increase intensity enhancement (and decrease threshold) by a factor of 2 [7, 11]; temperature dependences and uncertainties in parameters due to poorly defined chemical composition and size effects, etc.

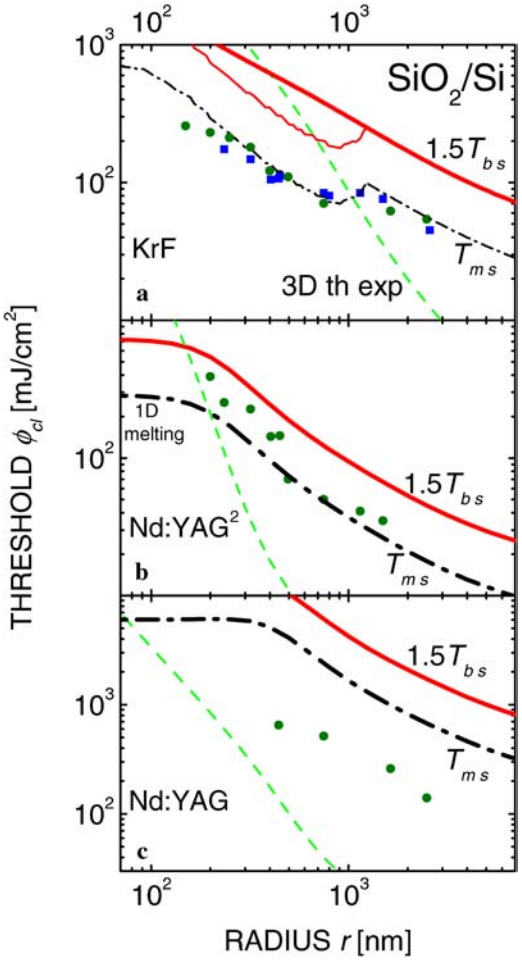

FIGURE 3 Theoretical and experimental values for the cleaning thresholds of SiO_2 particles from Si at different wavelength. *Solid curve* – threshold based on the evaporation of the substrate. *Dashed curve* – threshold based on the 3D thermal expansion of the substrate and particle. *Dash-dotted* curve refers to a local melting of the substrate. **a** $\lambda = 248$ nm. *Thin solid curve* uses exact averaged Mie results from Fig. 2. Experimental data: *squares* and *circles*. The latter set was obtained under the controlled heating (3 h) and storage time (< 24 h) conditions. **b** $\lambda = 532$ nm. Experimental points are taken from [3]. **c** $\lambda = 1064$ nm

The theoretical melting curve may serve as an upper limit for 'damage free cleaning'. For small particles it approaches the homogeneous melting threshold, while for large ones it decreases strongly.

The larger discrepancy for the 1064 nm radiation (Fig. 3c) is probably due to the strong temperature dependence of absorption coefficient at this wavelength. The ablative cleaning model (unlike 3D thermal expansion model), yields reasonable slope of the $\phi_{\rm cl}(r)$ dependence for all three cases.

Damage under the particles was always observed experimentally for the case of 532 nm and 1064 nm radiation. It was claimed in [15] that cleaning threshold (for polystyrene particles and 532 nm), coincides with that of local ablation. With 248 nm damage was found near the threshold for $2r > 3000$ nm, and at the fluences twice above threshold for $2r > 1500$ nm. For smaller particles at such fluences no damage was observed with dark field microscope, SEM or AFM. However, the amount of ablated material can be so small, that it is difficult to register damage.

7 Influence of ambient humidity

The cleaning in humid atmosphere was mentioned in [15, 17]. Water meniscus is formed between the particle and the substrate due to capillary condensation. The volume of the capillary condensed water for complete wetting is about $V_l \approx 4\pi R_{\rm K}^2 r$ where Kelvin radius $R_{\rm K}$ can be expressed via gas constant $R_{\rm G}$, density ϱ_l, molar weight μ and surface tension coefficient σ of the liquid:

$$R_{\rm K} \approx \frac{\mu\sigma}{\varrho_l R_{\rm G} T \ln(RH^{-1})} = \frac{0.52\,\text{nm}}{\ln(RH^{-1})}\,. \tag{6}$$

The cleaning conditions can be understood along the lines similar to those of ablative cleaning. There exist, however, certain differences. Critical temperature $T_{\rm cl}$ of water is low, so that with large overheating water will vaporize explosively. Unless RH is close to 1, $R_{\rm K}$ and V_l are rather small and condensed water may not contribute significantly to the removal of large particles. Thus, for RH cleaning one has to have enough water and to heat it 'well above' $T_{\rm cl}$. Figure 4 shows cleaning thresholds measured in vacuum and with high $RH = 94\%$–97% together with the calculated fluence necessary to achieve substrate evaporation, melting and critical temperature of water. The calculations were performed as in Sects. 2–6 (without exact Mie results) and did not include the influence of water on optical or thermal problem.

High RH improves cleaning of particles with $r < 300$ nm, and increases cleaning threshold for larger particles. The values of the RH thresholds gradually deviate from the curve corresponding to melting or evaporation of the substrate, to the dashed curve corresponding to the critical temperature of water. This suggests the following scenario: Water condensate does not change the cleaning mechanism, but gradually

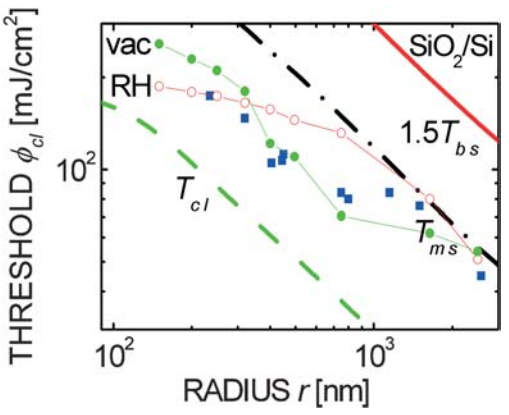

FIGURE 4 Comparison between the cleaning thresholds at 248 nm in vacuum (*filled symbols*, the same as in Fig. 3a) and in $RH = 94\%$–97% (*open circles*). *Solid curve* – threshold based on the evaporation of the substrate, *dashed curve* – threshold based on the critical temperature for water. *Dash-dotted curve* – melting of the substrate

contributes to the cleaning force. Its contribution becomes significant when the volume (or radius) of condensate is comparable with that of ablated material. Using estimation for V_l from above and w_g from (4) we get:

$$4\pi R_K^2 r > \pi w_g^2 h \Rightarrow r < \frac{4R_K^2}{h}\frac{27n^4}{(4-n^2)^3}$$

or, comparing the radii,

$$2\sqrt{rR_K} > w_g \Rightarrow r < 4R_K\frac{27n^4}{(4-n^2)^3} \tag{7}$$

$R_K(RH = 0.95) = 10$ nm, and with $h = 10$ nm, both estimations yield $r < 0.5$–1 μm for $n = 1.4 - 1.5$. This is in qualitative agreement with the experimental results in Fig. 4.

It is unclear why cleaning threshold increases for average-sized particles. If they are cleaned via a thermal expansion mechanism, capillary condensation may increase threshold via capillary force. For an ablative cleaning mechanism this is irrelevant, as the water shall evaporate before the cleaning starts. This seems to be the case for the particles with $2r > 3000$ nm, where the damage was always observed. Water may also weaken focusing of radiation. Besides, if the evaporation of the water alone does not start particle removal, the energy spent on its evaporation will be spent in vain. Similar experiments with the Nd : YAG laser did not reveal significant difference between the vacuum and RH cleaning.

8 Principal limitations for damage-free DLC based on thermal expansion

The damage threshold is determined by the surface temperature, while the thermal expansion l (which is the driving force for damage-free DLC) by the integral of this temperature over the heated depth. For weak absorbers the latter is determined by the absorption length. Thus, a wavelength with weaker substrate absorption may be advantageous for DLC. This was the rationale behind the Nd : YAG cleaning experiments presented above.

We will discuss the limit of particles with $r \ll \lambda$. For cleaning in microelectronics, micromechanics, etc., particles that cannot be removed by conventional methods are typically below 100 nm in size. Field enhancement becomes less pronounced for such particles. Small particles are removed in force regime [6, 7] $-m\ddot{l} \sim ml/\tau^2 > F_0$. The temperature rise at the surface should not exceed that of melting, ΔT_{ms}. The biggest expansion can be achieved with the largest depth of expanding material. In the most favorable 1D case without radial 3D heat conduction [8], heated depth can be approximated as the sum of absorption and thermal lengths l_α and l_T [1]. With the shorter pulses this is the former. Thus, the maximum damage-free thermal expansion can be approximated as $l_{\max} \approx \beta_1 \Delta T_{ms}(l_\alpha + l_T)$, where $\beta_1 = \frac{1+\sigma_s}{1-\sigma_s}\frac{\beta_s}{3}$ is the (1D) coefficient of thermal expansion [6, 7]. Combining this with the force removal criterion, we get the margins for expansion l that ensure damage-free cleaning:

$$\beta_1 \Delta T_{ms}(l_\alpha + l_T) > l > \xi_1 \frac{F_0(r)\tau^2}{m(r)}\,. \tag{8}$$

Here and below $\xi_i \sim 1$ are dimensionless coefficients depending on the approximations used. Resolving this inequality for r we get the restriction on the sizes of particles that can be removed without damage. For FWHM τ_F we assume $\tau = 0.41\tau_F$.

$$r > \xi_2 \left(\frac{\varphi}{\varrho_p \beta_1 \Delta T_{ms}}\right)^{1/2} \frac{\tau_F}{(l_\alpha + \xi_3\sqrt{D_s\tau_F})^{1/2}}$$
$$\approx \frac{0.1\tau_F}{(l_\alpha + 0.16\sqrt{\tau_F})^{1/2}}\,. \tag{9}$$

The last equality is written for SiO_2/Si using values from the Table 2 with $\xi_1 = e^2$, $\xi_2 = 0.41(3e^2/2)^{1/2} = 1.37$, $\xi_3 = \sqrt{\pi}/2 \approx 0.89$ (see [1, 7]). It assumes that r and l_α measured in μm and extit τ_F in ns. The family of such curves is presented in Fig. 5. In addition we require $l_\alpha + l_T < v_0\tau_F$, so that the finite speed of sound v_0 does not decrease the rate of thermal expansion [18]. This estimates the limit of removable size for the 1D DLC mechanism: $r > 0.032\sqrt{\tau_F}$ (dashed line). One can see that excimer lasers are not ideally suited for the cleaning of sub-μm particles due to their strong absorption and long pulse duration (upper corner bounded by the thick solid and dotted line). The most suitable seem to be 10–100 ps pulses with $l_\alpha \sim 0.1$–1 μm (dash-dotted curves). For Si this suggests the usage of IR lasers with $\lambda \sim 5$–10 μm, especially at high doping levels and temperatures where absorption length shrinks into μm range. In addition, longer wavelength decreases Mie parameter kr and therefore the field enhancement.

9 Conclusions

Theoretical analysis of DLC experiments at three different laser wavelength shows that the model based on local ablation describes the slope of fluence vs. size threshold curves better than the model based on the (3D) thermal expansion. Nevertheless, exact correspondence with the experiments cannot be achieved.

Quantitative comparison of the theory with experiment requires full-fledged numerical 3D calculations, which take into account temperature dependences of thermo-physical, optical and adhesion parameters of the substrate and particle, as well as changes in geometry during the laser pulse.

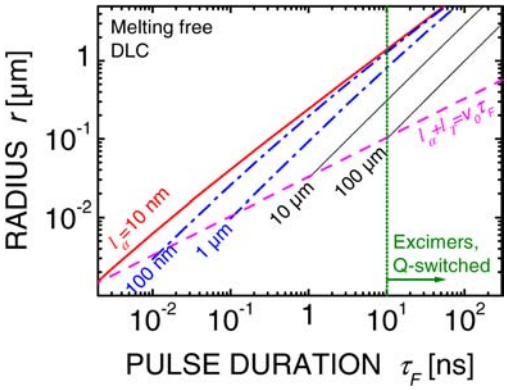

FIGURE 5 Limits for damage-free DLC as a function of FWHM pulse duration. *Curves* are indexed by the absorption length in the substrate as described in (4). *Dotted curve* indicates the duration of the typical excimer and Q-switched lasers. *Dashed curve* indicates the onset of the decrease in thermal expansion rate due to finite sound velocity

High *RH* improves cleaning of small particles, hinders that of particles with 600 nm $< 2r <$ 3 μm, and has no effect on larger ones. This is attributed to the gradual contribution of the capillary condensed water to the ablative cleaning mechanism.

One can try to avoid damage associated with the local intensity enhancement by shifting cleaning laser wavelength into IR region where absorption of Si substrate is weaker, and Mie parameter kr responsible for the intensity enhancement is lower.

ACKNOWLEDGEMENTS We thank Dipl. Ing. M. Mosbacher and Prof. B. Luk'yanchuk for useful discussions and Dr. Z. B. Wang for the program used for Mie calculations. Financial support was provided by the Fonds zur Förderung der wissenschaftlichen Forschung in Österreich, project P14700-TPH.

REFERENCES

1 D. Bäuerle: *Laser Processing and Chemistry*, 3rd ed. (Springer, Berlin 2000)
2 Y.F. Lu, Y.W. Zheng, W.D. Song: Appl. Phys. A **68** 569 (1999)
3 N. Arnold, G. Schrems, T. Mühlberger, M. Bertsch, M. Mosbacher, P. Leiderer, D. Bäuerle: Proc. SPIE **4426**, 340 (2002)
4 M. Arronte, P. Neves, R. Vilar: J. Appl. Phys. **92**(12) 6973 (2002)
5 B. S. Luk'yanchuk, Y.W. Zheng, Y.F. Lu: Proc. SPIE **4423**, 115 (2001)
6 N. Arnold: Appl. Surf. Sci. **208–209**, 15 (2003)
7 *Laser Cleaning*, ed. by B. Luk'yanchuk (World Scientific, New Jersey, London 2002) Chapt. 2, 3
8 B. Luk'yanchuk, N. Arnold, S.M. Huang, Z.B. Wang, M.H. Hong: Appl. Phys. A **77**(2), 209 (2003)
9 H.-J. Münzer, M. Mosbacher, M. Bertsch, O. Dubbers, A. Pack, R. Wannemacher, B.-U. Runge, D. Bäuerle, P. Leiderer: Proc. SPIE **4426**, 180 (2002)
10 H.-J. Münzer, M. Mosbacher, M. Bertsch, J. Zimmermann, P. Leiderer, J. Boneberg: Journal of Microscopy **202**, 129 (2001)
11 B. S. Luk'yanchuk, Y.W. Zheng, Y.F. Lu: Proc. SPIE **4065**, 576 (2000)
12 Yu.A. Kravtsov, Yu.I. Orlov: *Caustics, catastrophes and wave fields* 2nd ed. (Springer, Berlin 1998)
13 N. Arnold: Appl. Surf. Sci. **197–198**, 904 (2002)
14 C.E. Bohren, D.R. Huffman: *Absorption and Scattering of Light by Small Particles* (John Willey & Sons, 1983) p. 169
15 M. Mosbacher, M. Bertsch, H.-J. Muenzer, V. Dobler, B.-U. Runge, D. Bäuerle, J. Boneberg, P. Leiderer: Proc. SPIE, **4426**, 308 (2002); M. Mosbacher, H.-J. Münzer, M. Bertsch, V. Dobler, N. Chaoui, J. Siegel, R. Oltra, D. Bäuerle, J. Boneberg, P. Leiderer, In *Particles on Surfaces 7*, ed. by K.L. Mittal (VSP Press, Netherlands 2002)
16 G. Vereecke, E. Röhr, M.M. Heyns: J. Appl. Phys. **85**, 3837 (1999)
17 T. Fourrier, G. Schrems, T. Mühlberger, J. Heitz, M. Mosbacher, J. Boneberg, P. Leiderer, N. Arnold, D. Bäuerle: Appl. Phys. A **72**, 1 (2001)
18 S. Pleasants, N. Arnold, D. Kane: Appl. Phys. A **79**, 507 (2004)
19 G. Schrems: Ph.D. Thesis (J.-Kepler-University, Linz 2003)